KERNFORSCHUNGSANLAGE JÜLICH GmbH

Institut für Plasmaphysik
Association EURATOM - KFA

Origin of Impurities in Hydrogen Plasmas

by

K. J. Dietz, F. Waelbroeck, P. Wienhold

Jül - 1448
August 1977

Als Manuskript gedruckt
ISSN 0366-0885

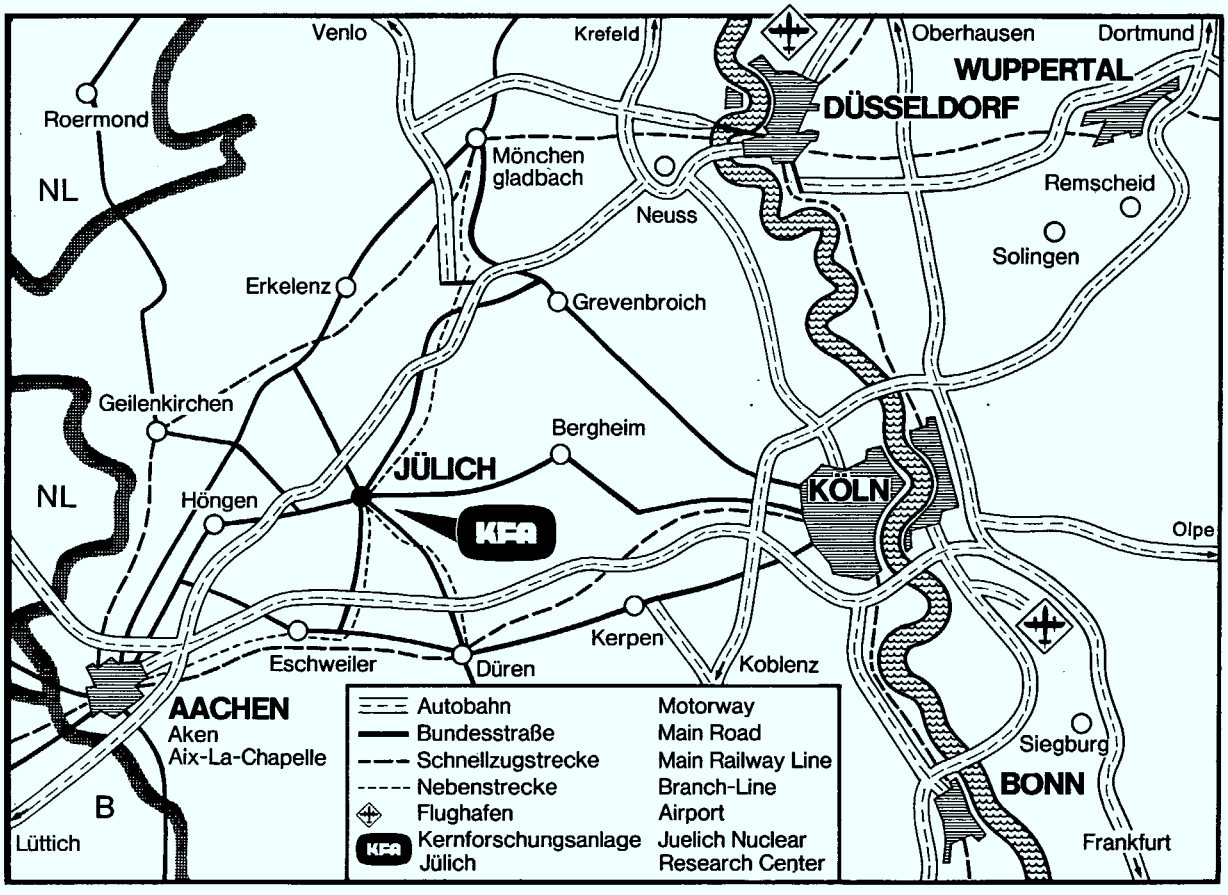

Berichte der Kernforschungsanlage Jülich – Nr. 1448

Institut für Plasmaphysik Jül – 1448

Im Tausch zu beziehen durch: ZENTRALBIBLIOTHEK der Kernforschungsanlage Jülich GmbH, Jülich, Bundesrepublik Deutschland

Origin of Impurities in Hydrogen Plasmas

by

K. J. Dietz, F. Waelbroeck, P. Wienhold

ORIGIN OF IMPURITIES IN HYDROGEN PLASMAS

K.J. Dietz, F. Waelbroeck, P. Wienhold
Institut für Plasmaphysik der Kernforschungsanlage Jülich GmbH
Association EURATOM/KFA

Summary

Prehandling and discharge cleaning methods applied in toroidal magnetic systems with metallic walls have been surveyed and their efficiency in depressing the initial concentration of low Z contaminants (mainly oxygen, but also carbon) have been compared. Chemical reactions between atomic (H^0 and H^+) hydrogen species and chemically bound oxygen and lattice-bound carbon in the surface-near layers are found to play a dominant role in the impurity release. Discharge cleaning in Tokamaks tends to crack and ionize the resulting water and hydrocarbons, leading to impurity ions which recombine chemically with the walls at the end of the discharge cycle.

An ultrahigh vacuum apparatus has been built, in which the cleaning efficiency of H^0 and H^+ is investigated. The flux densities of the atomic species have been varied between 10^{14} and 5×10^{16} atoms/cm^{2}s, covering the range of the averaged values of present day confinement devices and future reactors. The cleaning efficiency is found to be high. A chemical kinetics model describes the mechanisms involved.

An H_2 blistering-like effect is observed and is attributed to the H + H recombination underneath the surface. This process influences the recycling phenomena and probably also accounts for the early appearance of metallic impurities in tokamak experiments.

Conclusions to be shown from our measurements concerning phenomena observed in confinement systems are presented.

I. Introduction

Oxygen and carbon, but also smaller amounts of heavier ions of limiter and wall materials are observed early in Tokamak discharges, at times when the ion and wall temperatures are too low to invoke sputtering or evaporation effects. To identify the mechanisms responsible for the appearance of these impurities, the efficiency of the prehandling and discharge cleaning procedures used in toroidal confinement devices has been surveyed within the framework of the TEXTOR programme on plasma-wall interaction. The most probable source of light impurities was found to be the chemical reactions of hydrogen atoms and atomic ions, generated during the discharge, with wall contaminants (adsorbed species) and wall constituents like oxides and lattice-bound carbon. These are highly enriched [1,2,3] in the surface near region and are not removed by heat treatments, which only release weakly bound species (adsorbed water, carbon oxide or other gases). Ion sputtering using for instance ions of N, Ne, Ar, can detach particles from the surfacenear region. These, however, recondense on other parts of the vessel before being pumped.

Cleaning discharges and main discharges in hydrogen produce Frank-Condon atoms during break-down and, later, as a consequence of recycling. Additional wall bombardment by outward diffusing atomic ions and neutrals occurs during and at the end of the discharge. The atomic and ionic species penetrate into and diffuse in the metal wall [4, 5, 6, 7]. They react with the bound carbon and oxygen present in the surface and form volatile methane, other hydrocarbons, and water. Carbon oxide and carbon dioxide are also formed if carbonates are present in the surface. In high current cleaning discharges of long duration, these species enter into the plasma of the discharge channel, where they are dissociated and ionized. At the end of the pulse, the C^{n+} and O^{m+} ions recombine chemically with the wall material. A small fraction of the impurity atoms released from the walls remains in the form of volatile products which can be pumped away. These are probably the products of chemical reactions occuring at the end of the discharge which are no longer cracked or ionized. The frequency of quenching phases should

therefore be more important to the efficiency of the cleaning procedure than the duration, or the power.
This is confirmed by the low Z_{eff} values achieved in W II b [8], W VII [9] and WEGA [10] by 50 Hz, and especially in ALCATOR [11] by 5 kHz discharge-cleaning. A further improvement is expected if the plasma electron temperature is low during the cleaning discharge as is the case in short discharges of low current at low B_T fields. Cracking and ionization of the molecules released become then less probable and a large amount of the H and H^+ procuded during the discharges contributes to the cleaning effect. This is expected to be the case in ALCATOR and to some extent also in W II b. The relatively low H_2 pressures ($\approx 10^{-4}$ Torr) at which toroidal discharges can be struck set however a limit to the achievable cleaning rates [12] .

These considerations have led us to investigate the cleaning of walls by hydrogen atoms and ions using well known techniques of producing H and H^+. These achieve high fluxes of atomic species and lead moreover, to a low or negligible probability of cracking and ionizing the volatile compounds released. The following criteria have guided the choices of the systems used:

- Modest local requirements to facilitate the introduction into existing or projected machines.
- Low power requirements to allow continuous operation during the cleaning procedure without overheating the surrounding walls.
- High cleaning rates for the first cleaning and later for the elimination surface layers which may appear during a prolonged shutdown as a consequence of residual leaks, oil from the vacuum system, or volume diffision of impurities.

In the following the experimental set-up is described. The experimental results are presented and discussed. In the conclusions, impacts of the results on the field of impurity generation will be presented.

II. Apparatus

Hot tungsten filaments, r-f and glow discharges in hydrogen up to pressures of one Torr are used to produce hydrogen atoms and

atomic ions. To detect the products of the reactions between the atomic species and the wall of the vacuum chamber, a quadrupole mass analyzer (QMA) is installed. Its maximum working pressure is to 10^{-4} Torr; it is therefore differentially pumped.

The experimental set up is shown in fig. 1. It consists of a cylindrical main vessel (MV) of 40 cm diameter and 100 cm length, evacuated by a turbomolecular pump (pumping speed at the vessel $\approx$ 140 l/s at 10^{-3} Torr). To dissociate H_2 an ohmically heated "squirrel cage" array of 20 tungsten wires (0.15 mm Ø, 22.5 cm length) and a stainless steel r-f coil (2 cm Ø, 12.5 windings, 3.5 cm length) are built into the MV. The electrical potential of both systems with respect to the MV can be varied. A liquid nitrogen cooled finger of 3000 cm^2 area inhibits the water-vapour catalysed transport of tungsten from the hot filaments [13] . The differentially pumped "quadrupole by-pass" (QBP) with a characteristic pumping time of 0.13 s is connected to the MV via an adjustable throttle.

The material used for the MV is SS 1.4541 (equivalent to SS 321) for the QBP SS 1.4301 (equivalent to SS 304). The vacuum system is bakeable up to 400° C.

III. Experimental

The QBP and the MV have first been baked for 72 hours up to 400°C. After baking the base pressure in the QBP was $\leq 10^{-9}$ Torr, leakage rate $\leq 6 \times 10^{-10}$ Torr l s^{-1}.

To measure the production rates, the walls of the MV and the QBP were first maintained at 150 - 180° C. With the tungsten filaments cold and without discharge 99.999% pure hydrogen was introduced into the MV at a pressure of 10^{-2} Torr. By adjusting the throttle the pressure in the QBP was then brought up to 10^{-5} Torr. Simultaneously an increase of the partial pressures of the masses 15, 18, 27 and 28 was observed. This results from the reactions of H-atoms and ions produced by the QMA ion source and the ionization

gauge and their subsequent reaction with impurities in the surface of the QBP walls. Thus processes in the MV, occuring after the activation of the hot filaments or the discharges could be partially masked. It was decided to clean first the QBP walls and to investigate the QBP wall cleaning in detail and then to study the MV cleaning.

IV. Results

The following notations are used:

V_m : Amplitude of the QMA signal corresponding to the mass m

V_m^o : Quasistationary value of V_m during evacuation

V_m^p : Quasistationary value of V_m for a hydrogen pressure p_{H_2}

$V_m^p(t)$: Time dependent value of V_m after changing the hydrogen pressure to p at the time t = 0

$\Delta V_m^p = V_m^p - V_m^o$

A. Dependence of signal amplitudes on the hydrogen pressure

In the QBP which had been only exposed to the residual hydrogen released during bake-out, the hydrogen pressure was raised stepwise to $5{,}5 \times 10^{-5}$ Torr. A variation of V_m (m = 15, 18, 27, 28) results. The quasistationary values V_m^p are reached in approximately 30 min. after a pressure change. This time decreases with increasing wall temperature and depends on the substance examined. V_m^p was found to be proportional to p_{H_2} as shown in fig. 2.

After the stepwise increase of p_{H_2}, the hydrogen pressure was increased to 1.4×10^{-4} Torr for 90 min. After reducing the pressure to 2.2×10^{-5} Torr the V_m^p values (marked in fig. 2) lie above the curve obtained with increasing pressure steps. Thus the phenomenon has hysterisis.

B. Time evolution of the signal amplitudes

In the QBP at a wall temperature of $\approx 300\ ^{o}C$ the hydrogen pressure was raised to 2×10^{-5} Torr and the temporal behaviour of the water partial pressure was observed using V_{17} (proportional to V_{18}).

The time evolution of V_{17} occurs in two stages as shown in fig. 3. An almost instaneous rise to V_{17} (t_1) is folled by a slow exponential evolution towards the quasi-equilibrium value V_{17}^p. The heights of the step, $\Delta V_{17} = V_{17}(t_1) - V_{17}^o$ is comparable to the half of the maximum increase $\Delta V_{17}^p = V_{17}^p - V_{17}^o$. For the masses m = 15, 27 and 28 a similar behaviour is found.

The measurements as reported above were repeated for wall temperatures of 150 - 180 °C after a preceeding intense wall bombardment with H-atoms and ions ($\approx 6.5 \times 10^{18}$ cm^{-2}). During the subsequent pump down in the course of which V_{17}^o decreases, hydrogen of a pressure of $2{,}25 \times 10^{-5}$ Torr was periodically introduced into the system. Each period had a duration of 30 min., followed by a pump down time of one hour. For each period the ΔV_m^p values were evaluated for m = 15, 17, 27 and 28 and were found to decrease with decreasing V_m^o. Furthermore, also the ratios $\Delta V_m/V_m^o$ and $V_m/\Delta V_m^p$ became smaller as V_m^o decreases.

C. Temporal behaviour of hydrogen

The hydrogen pressure in the QBP was maintained at 10^{-2} Torr for 18 hours using the ion gauge to produce hydrogen atoms and ions with a flux density of $\approx 10^{13}$ $cm^{-2}s^{-1}$.

After evacuation the pressure did not drop back to its initial value of 10^{-9} Torr but only to 10^{-6} Torr. Thereafter it decreased slowly to 2×10^{-7} Torr in several hours and to 2×10^{-8} Torr in days. The residual gas analysis showed the pressure to be mainly due to H_2, but also the H_2O, m = 28, CH_4 and other hydrocarbon partial pressures were larger than before the treatment. The water partial pressure decreased more rapidly than the total pressure (mostly hydrogen), but the characteristic time was of the order of hours. The total pressure as well as the hydrogen pressure (and to a smaller extent CH_3^+), as shown fluctuate (fig. 4) in phase during the pump down. This indicates the liberation of many bursts of gas per second, and this during days.

After introducing N_2 at 760 Torr for two minutes into the QBP and a subsequent pumpdown, the total pressure dropped after some seconds to $\approx 10^{-9}$ Torr, its initial value before the treatment

with hydrogen. Occasioanlly large pressure spikes, corresponding to large H_2 bursts are observed. Exposing the surface to a flux of atomic hydrogen ($\approx 3x10^{13} cm^{-2} s^{-1}$) for five minutes brought back the sporadic hydrogen emission to its former value.

D. Cleaning of the QBP

The treatment of the QBP at a temperature of 350 °C with doses of atomic hydrogen of $\approx 6{,}5 \times 10^{18}$ cm^{-2} resulted in a depression of the sources of C and O.

Extrapolating the water production for a treatment at $p_{H_2} = 10^{-2}$ Torr, one evaluates that during the treatment $\approx 5 \times 10^{17}$ water molecules per cm^{-2} i.e. several hundred of monolayers have been released.

Residual masses like m = 19 (F^+), 35 and 37 (Cl^+) which could not be appreciably reduced even after one week of pumping at wall temperatures between 150 °C and 400 °C, had been depressed by more than one order of magnitude. These masses originate probably from the $C_2Cl_3F_3$ used as a final cleaning liquid for the vacuum sufaces.

After a treatment of the walls at T = 350 °C for 72 hours with $\approx 2 \times 10^{19}$ hydrogen atoms per cm^2 the initial reducible oxygen content in the wall decreased by a factor of 10^4.

E. Measurements in the Main Vessel

The cleaning of the QBP being terminated, the production rates for the masses m = 15 (CH_3^+), 17 (OH^+), 28 (CO^+) and 44 (CO_2^+) are measured in the MV, using the hot filament, the r-f and the glow discharges to produce atomic hydrogen species. To measure the water production, the liquid nitrogen cooled finger was not operated . Thus a water vapour catalyzed transport of tungsten [13] using the hot filament was not avoided during this measurement (40 min). From the observation o: of the partial pressures of the different masses in the QBP the production rates in the MV could be calculated knowing the pumping speeds and the conductances. In the QBP not only the turbomolecular pump but also the walls, which are activated by the previous clean-

ing, pump. The resulting pumping speed which depends on the substance considered is not known but it could be established that, for water, it is much larger than that of turbo-molecular pump. For the calculation of the production rates only the pumping speed of the turbomolecular pump was taken into account. Thus the production rates evaluated and presented in table 1 are lower limits. Additionally the production rates decrease with time, due to the advanced wall cleaning during the measurements, which are carried out in that order as shown in table 1. The columns present the method applied, the time averaged electrical power needed, the wall temperatures, the pressures at which the measurements are carried out, the production rates for the different masses and in the last two columns the total amount of removed carbon and oxygen.

In the last three rows a comparison is made with the TFR cleaning as measured earlier [12] . The time averaged pumped impurities are calculated as production rates for the cleaning. From these values it is not possible to obtain the impurity content in the discharge because of the strong pumping of the walls after the discharge especially for water and carbon oxides. Thus only a fraction of them is pumped and contributes to the production rates for the wall cleaning.

As it is seen from the table the most efficient method for the cleaning is a combination of r-f and glow discharge. At higher current densities dissociation of the gaseous impurities occurs as it is seen for the production rates of water.

Compared to the normal operation of TFR, i.e. four hours cleaning discharges and ten hours main discharges a day four days a weeks, the cleaning rate of one year of operation without opening the machine corresponds to three days of continuous operation of a glow and r-f discharge at a pressure of 9.5×10^{-2} Torr and a current density of 10 $\mu A/cm^2$.

V. Discussion of the experimental results

A. Hydrogen flux densities

The production rate, N_H of hydrogen atoms by dissociation of molecules on a tungsten filament of unit area $[cm^2]$ at the temperature T_{fil} is given by [14]

$$N_H = \frac{k_A}{k_r}\left[- k_A + (k_A^2 + n\bar{v}s \cdot k_r)^{1/2} \right] \text{ atoms/cm}^2\text{s} \qquad (1)$$

where the rate of atomization $k_A = 2{,}2 \times 10^{13} \exp(-67/RT_{fil})\ [s^{-1}]$ and the rate of H_2 evaporation $k_r = 5 \times 10^{-3} \exp(-31/RT_{fil})\ [s^{-1}]$ (activation energies in kcal/mol).

$1/4\ n\ \bar{v}$ is the number of molecules with the mean velocity $\bar{v}$ impinging on the surface, the sticking probability $s = 0{,}37$ [15]. The production rate of hydrogen atoms for the squirrel cage as a function of the hydrogen pressure is shown in fig. 5.

For pressures below 5×10^{-4} Torr N_H is proportional to p_{H_2}, whereas at higher pressures it is proportional to the square root of the pressure.

Since recombination into molecules in the gas requires a three-body process, which is unlikely at intermediate pressures, the system can operate in the diffusion domain; i.e. at higher pressures H atoms can to some extent diffuse around corners.

A small correction for the mean velocity $\bar{v}$, depending on the ratio filament diameter D_f to the mean free path λ of H_2, should be applied to (1). It is of the order $(T_w/T_{fil})^{1/2}$ in the limiting case $D_f/\lambda \to \infty$. Neglecting this factor we obtain for the squirrel cage:

$T_w = 422$ K, $T_{fil} = 2000$ K, $p_{H_2} = 1$ Torr, $S_f \approx 20$ cm^2,

$$N_H \cdot S_f = 7{,}3 \times 10^{20} \quad \text{atoms/s}$$

The surrounding area is $S \approx 1{,}5 \times 10^4$ cm^2 and the maximum flux density φ_H of H atoms at the wall should reach

$$\varphi_H = 4{,}8 \times 10^{16} \quad \text{atoms/cm}^2\text{s}.$$

That is about ten times larger than expected in a 5 GW_{th} Tokamak reactor with a duty cycle of one, a minor radius of 300 cm, an average density of 2×10^{14} cm^{-3}, and a particle confinement time (α-removal) of 10 s.

An estimate of the formation of atomic hydrogen species in the QBP showed that the most efficient source is the dissociation of hydrogen molecules on the tungsten filament of the QMA. The production of ionic species is smaller by three orders of magnitude. The flux densities of hydrogen atoms as a function of the hydrogen pressure was calculated taking into account the geometry of the QMA ion source and the influence of the mean free path of the hydrogen atoms. For $\lambda > D_{QBP}$, the diameter of the QBP, the transport of hydrogen atoms is molecular, only a fraction (≈ 10 %) of the surface is attacked.

For $\lambda < D_{QBP}$ the transport is diffusive. The result of the calculations is shown in fig. 6. The two limiting cases are indicated by the lines. The intermediate regime is extrapolated and represented by the dashed line. It should be noted that the flux density of atomic hydrogen is proportional to the pressure up to $\approx 10^{-4}$ Torr. In the QBP, according to fig. 6, the flux density of hydrogen atoms at $p_{H_2} = 10^{-2}$ Torr is given by

$$\varphi_H = 1{,}2 \times 10^{14} \text{ atoms/cm}^2\text{s}$$

In present-day Tokamak discharges, φ_H is of the order of 5×10^{15} (atoms + ions) cm^{-2}s^{-1}, but the duty cycle is low ($\approx 1/100$); thus the time-averaged fluxes in QBP and these devices are comparable.

B. Hydrogen behaviour at the wall

During the treatment the hydrogen is adsorbed on and penetrates into the metal. A fraction Φ_{in} of the impinging flux is trapped.

$$\Phi_{in} = w\, S\, \varphi_H \qquad (2)$$

where w is the probability for a hydrogen atom to stick at the wall and S the surface of the wall.

The outgoing flux Φ_{out} of hydrogen molecules results from recombination of hydrogen atoms on the surface and from atoms having diffused to the surface and recombining with a surface atom.

$$\Phi_{out} = S\,(k_r\, n^2 + k_r'\, c_1\, n) \qquad (3)$$

where k_r and k_r' are the recombination rates for both processes, n the surface density of hydrogen atoms and c_1 the concentration in the bulk.

Small fluxes of φ_H are considered, thus the recombination of impinging atoms with wall atoms is neglected. Equilibrium between surface and bulk atoms is assumed (Henry's law) leading to

$$c_1 = k_s\, n \qquad (4)$$

where k_s is the proportionality constant, which is only temperature dependent.

In the quasistationary state

$$\Phi_{in} = 2\,\Phi_{out} \qquad (5)$$

As shown in fig. 6, φ_H is proportional to p_{H_2} for pressures below 10^{-4} Torr. This lead to the expression

$$c_1 \propto p_{H_2}^{1/2} \qquad (6)$$

The concentration c_1 of atoms in the wall ($T \approx 150\ ^{o}C$) during and after the treatment is largely oversaturated with respect to the outer H_2 pressure [16]. The atoms partly recombine to H_2 underneath the surface in lattice defects and grain boundaries, leading to H_2 molecules with a low solubility and low diffusion velocity. These accumulate, forming pockets and can thereafter released in a blister-like mechanism [17, 18, 19, 20, 21].

C. Water production rates

The reaction of hydrogen atoms with contaminants and constituents of the metallic walls are explained by a chemical model. As an example a possible, probably not unique, reaction scheme for the formation of water is presented.

The hydrogen atoms react with a reducible metal oxide MO with the concentration c_{MO} in the bulk. The reaction rates v are proportional to the concentrations of the reactants, with the temperature dependent reaction constants k.

$$MO + H \longrightarrow MOH \qquad v_{MOH} = k_{MOH}\, c_{MO}\, c_1 \tag{7a}$$

$$MOH \longrightarrow MO + H \qquad v_{MO} = k_{MO}\, c_{MOH} \tag{7b}$$

$$MOH + H \longrightarrow ** \longrightarrow M + H_2O \qquad v_{18} = k_{18}\, c_{MOH} \cdot c_1 \tag{7c}$$

assuming quasi-equilibrium for (7a) and (7b) results in

$$v_{18} \ll v_{MOH} \approx v_{MO} \tag{7d}$$

and

$$c_{MOH} \approx k\, c_{MO}\, c_1$$

with

$$k = \frac{k_{MOH}}{k_{MO}}$$

As observed experimentally, during the treatment at the pressure p V_{18} reaches a stationary value V_{18}^{p}, which is proportional to v_{18}. The water production in the volume Ω is given by

$$V_{18} = \int_{\Omega} k_{18}\, c_{MOH}\, c_1\, d\Omega = \int_{\Omega} k_{18}\, k\, c_{MO} (c_1^{p})^2\, d\Omega \propto V_{18}^{p} \tag{8}$$

or

$$V_{18}^{p} \approx \frac{1}{K} K_{18}(T)\ c_{MO}\ c_1^{p} \approx K_{18}(T)\ c_{MO}\ (c_1^{p})^2 \qquad (9)$$

where

$$c_1^{p} = c_1^{o} + \Delta c_1 \qquad (10)$$

the sum of the initially present hydrogen c_1^{o} and the hydrogen Δc_1 due to the treatment. One obtains

$$\Delta V_{18}^{p} = V_{18}^{p} - V_{18}^{o} = K_{18}(T)\ c_{MO} \left[(c_1^{o} + \Delta c_1)^2 - (c_1^{o})^2 \right] \qquad (11)$$

The first measurements of the pressure dependence of V_m were carried out unter the condition

$$c_1^{o} \ll \Delta c_1$$

resulting in

$$V_{18}^{p} \approx K_{18}(T)\ c_{MO}\ (\Delta c_H)^2 \qquad (12)$$

For hydrogen pressures below 10^{-4} Torr according to (6)

$$V_{18}^{p} \propto p_{H_2}$$

in agreement with the observations (fig. 2).

The fact that the points denoted by in fig. 2 lie above the curve obtained during the stepwise pressure increase results probably from the increase of c_1^{o} which had occurred during the 90 minutes pretreatment at 1.5×10^{-4} Torr before the measurements at the lower pressures were carried out. For these measurements now eq. (11) holds and the production rates should be larger, as observed.

In the equations (7a) and (7b) quasi-equilibrium was assumed. This is necessary to explain the experimental results, otherwise one would have deduced

$$V_{18}^{p} \propto p_H^{1/2}$$

which is not observed.

The MO content is localized near the surface. In contrast to the H recombination which also occurs in deeper layers, the decay of the water signal after the treatment should then be faster than that of hydrogen. This is in agreement with the experimental results (ref. II. C)

D. The time evolution of the water production rates

As described in IV C. a two staged reaction rate is observed after raising the hydrogen pressure (fig. 3). This can be accounted for, in the above proposed scheme, as follows: a rapid increase of c_1 to its new quasi-equilibrium value c_1^p at $t_1 \approx 0$ increases the rate of step (7c) and thus V_{18} by

$$V_{18}(t_1) - V_{18}^o = K_{18}(T)\ c_{MO} \cdot c_1^o \cdot \Delta c_1 \qquad (13)$$

The initial concentration of MOH, $c_{MOH} = kc_{MO} \cdot c_1^o$, which is used for eq. (13) does not come immediately into equilibrium with the increased hydrogen concentration. The adjustment of c_{MOH} from its initial to its ultimate value is a slow process compared to the increase of c_1.

From the kinetics equations (7) follows:

$$\frac{d\ c_{MOH}}{dt} = k_{MOH}\ c_{MO}\ c_1^p - k_{MO}\ c_{MOH} - k_{18}\ c_{MOH} \cdot c_1^p \qquad (14)$$

The solution of this differential equation is, assuming c_{MO} and c_1^p to be time independent and $k_{MO} \gg k_{18}\ c_1^p$

$$c_{MOH}(t) = -k\ c_{MO} \cdot \Delta c_1 \cdot \exp(-k_{MO}t) + k\ c_{MO}\ c_1^p \qquad (15)$$

with

$\Delta c_1 = c_1^p - c_1^o$ and k from eq. (7d)

and finally with eq. (7c, 8, 9)

$$V_{18}(t) = V_{18}^p - \left[V_{18}^p - (V_{18}^o\ V_{18}^p)^{1/2} \right] \exp(-k_{MO}t) \qquad (16)$$

For the decay of the water production after decreasing the hydrogen pressure assuming an immediate decay of c_1 in the surface near region, a similar equation results.

In fig. 3 a comparison between the values obtained from eq. (16) with the experimental curve is shown. In the experiment $V_{17}(t)$ was measured, which is proportional to $V_{18}(t)$. For the calculation V_{17}^o and V_{17}^p were taken from the measurements. k_{MO} results from the slope of the semilogarithmic plot of $V_{17}^p - V_{17}(t)$. The good agreement of the calculated curve with the experimental points during the hydrogen treatment is a good evidence for the validity of a model as described in eq. (7). For the decrease of the signal, the experimental points lie above the calculated curve. This may be attributed to a decrease of the hydrogen concentration c_1 which is not infinitely fast compared to k_{MO}^{-1} and the assumption of an immediate decay of c_1 in the surface near layers is only an approximation.

E. The residual concentration of the impurities

Rising the p_{H_2} pressure in the presence of atomic hydrogen producing devices results in an increase of the hydrogen concentration in the solid. When quasi-equilibrium is attained, the new atomic hydrogen concentration c_1 in the solid is

$$c_1^p = c_1^o + \Delta c_1 \tag{10}$$

where c_1^o is the residual concentration before the test and Δc_1 the perturbation of c_1 resulting from the added "testing" H-atoms caused by the H_2 dissociation on the filament. Thus the quasi-stationary amplitudes of the m=18 peak, before the test phase V_{18}^o and after adding the test gas V_{18}^p are related by (using eq. (9)):

$$(V_{18}^p)^{1/2} = (V_{18}^o)^{1/2} + (A_{18})^{1/2} \tag{17}$$

where

$$A_{18} = K_{18}(T)\, c_{MO}\, (\Delta c_1)^2 \tag{18}$$

Since Δc_1 and the wall temperature are the same during all testing procedures, an unabmiguous comparison of the MO, concentrations before and after the cleaning procedure is obtained by evaluating A_{18}. In the presence of the V_{18}^o slowly decreasing background, which, according to eq. (11), does not allow to measure MO from the V_{18}^p signals, A_{18} can be derived by eq. (17).

F

Fig. 7 shows the plot of $(V_{17}^p)^{1/2} = f\,(V_{17}^o)^{1/2}$ obtained after a treatment. It checks the validity of equation (17) and confirms that (wall temperature = 150 °C), the <u>persisting volume reaction</u> and not the <u>wall desorption</u> dominates the H_2O release after the treatment. The points denotes 1, 2 are obtained in that order the next day during the test, indicating the deoxidation of the surface during the measurement.

From eq. (13) with eq. (18) one derives

$$\frac{V_{18}(t_1) - V_{18}^o}{(V_{18}^o)^{1/2}} = (A_{18})^{1/2} \qquad (19)$$

This is an independent measure for the metal oxide concentration. The good agreement of A_{18} computed from eq. (17) and (19) using the experimental values of fig. 3 and the relation $V_{18} = 3{,}82 \times V_{17}$, is a good evidence for the validity of the above described model.

Thus a set of rate equations such as (7) describes quantitatively <u>all</u> measurements made to date in our devices; their solution leads to different ways to determine the relative amount of MO in the surface as a function of the cleaning time.

Similar reaction schemes explain the results obtained for the production of other impurities. Again quasi-equilibrium has to be assumed for the first step of the processes, leading to kinetic equations in the form of eq. (16) and to values A_m which for constant temperature and constant hydrogen pressure are proportional to the concentration of the corresponding contaminant concentration in the solids.

With the reduced atomic-hydrogen fluxes used in the QBP, the C, O and other contaminant sources can be strongly depressed within a reasonably short time:

The following table gives the decrease of A_{15}, A_{18}, A_{27} and A_{28} observed in the QBP after 18 hours treatment with $\varphi_H = 10^{14}$ atoms/cm^2s.

	before treatment A_m (mV)	after treatment A_m (mV)	ratio
m = 15 (CH_3^+)	26	12.9	2
m = 18 (OH_2)	339.5	45.6	7.2
m = 27 ($C_2H_3^+$)	37.4	11.2	3.3
m = 28	35.1	13.7	2.6

The fact that oxygen is removed comparatively faster than carbon could result from a higher reaction velocity, but more probably from the finite thickness of the oxyde layer, whereas C is a constituant of the steel used here.

The decrease of the concentration of reducible bound oxygen (MO) by a factor 7, even using low φ_H values, should be underlined in view of the role which O^{m+} ions play as a contaminant in Tokamak devices.

VI. Conclusions

A. Cleaning of metallic walls by hydrogen atoms and ions

The formation of gaseous hydrogen compounds by the interaction of H^+ and H^o with stainless steel walls has been demonstrated. Agreement of the experimental results is found with a chemical kinetics model. This is a strong argument for the validity of the interpretation. Even with small fluxes of atomic hydrogen ($\varphi_H \approx 10^{14}$ atoms $cm^{-2}s^{-1}$) the impurities decrease in a reasonable short time: Residual vacuum pump oil after 3 hours, reducible oxides by a factor of 10^4 after 72 hours at T = 350 °C.

With higher fluxes $\varphi_H \approx 10^{16}$ atoms $cm^{-2}s^{-1}$ at wall temperatures of 220 °C the production rates of carbon and oxygen amount to 10^{11} $cm^{-2}s^{-1}$ using the tungsten filament to dissociate hydrogen.

With r-f and glow discharges at low power (130 Watt) the production rates are increased by more than one order of magnitude.

Using the cleaning devices at full efficiency the cleaning rates should still be increased by a factor of ten.

The methods discussed here are of great use to clean walls, among others of confinement devices, since the cleaning efficiency is high and the costs are low. They do not require to activate any special coil assembly and can in principle be introduced and retracted through any reasonable port-hole. They can be used quasi-continuously (power requirements of a few hundreds of watts) and the pressure operating domain is such that the hydrogen atoms can, up to a point, diffuse around corners.

The measurements indicate that it is misleading to attribute the water coming from the wall between Tokamak and other discharges to a desorption process, at least at wall temperatures of 150 °C. They show that the release can be quantitatively ascribed to the reaction of the residual metal oxyde with H atoms having diffused into the lattice during previous discharges. The same is true of CH_4, produced from lattice carbon the release of other contaminants and H_2.

The effects which play a decisive role here have a strongly non-linear dependence on the atomic hydrogen concentration c_1 in the solid. Some have threshhold values (oversaturation of H atoms, solubility of hydrogen molecules). They can only be simulated reasonably well when the flux densities of atomic species coming to the walls are of the same order of magnitude as those found in confinement devices; this is the case in our system.

B. Hydrogen behaviour

A problem results from the recombination of H atoms into H_2, and from the resulting pocket formation under the surface. Decarbonized stainless steel is very soft, and the release of

pockets occurs probably through a blistering process. This might lead to a steady "rainfall" of microscopic metallic dust particles through the vessel during long periods after exposure to H and H^+. Surface hardening (as was done here with N_2 after H treatment) can only partially alleviate the problem, since less frequent, but larger pockets still break up. In addition NH_3 production through H^o and H^+ leads to the disappearance of this effect.

Such metallic rainfall through the system might possibly build a mechanism for the early appearance of heavy ions (Mo in TFR, Fe in ST) in the oxygen poor discharges where H permeation into the metal is expected to be easy. This problem is being addressed in two notes showing the origin , methods of elimination of the effect and evidence for its existence [20, 21].

C. Consequences for confinement devices

The observations reported here show a considerable hysterisis and memory effect of the wall. The hydrogen dissolved in the solid decreases but very slowly. Similarly the phenomena occurring during one particular tokamak discharge are strongly influenced by the number, repetition rate and characteristic parameters of the preceeding discharges. This is in agreement with many observations in Tokamaks and Stellarators.

The hydrogen permeation appears to occur readily through surfaces which are not strongly oxydized. This explains the linear dependence of $V_m^p \propto p_{H_2}$ of fig. 1, which is only expected (eq. (6, 12) when c_1^o is very small. Also the different evolutions of $p_{H_2}(t)$ after discharges in TFR [12] and DITE [22], where $p \propto \exp(-kt)$ and $p \propto 1/t$ dependences are observed respectively.

If, as was done in DITE [23] , during a quasi-stationary phase in a discharge in hydrogen, a puff of deuterium is injected, an increase of the released hydrogen is expected. It may be assumed for example that the enhanced recycling leads to an atomic D concentration under, but near the surface which is equal to the

previous H atom concentration. The recombination rate and the resulting release of molecules (H_2, HD, DH, D_2) is increased, since $v_r = k_r (c_1+c_D)^2$. Thus a doubling of the H release rate results for this particular D_2 injection quantity.

The long-time mechanical behaviour of the first wall will be influenced by decarbonisation and corrosion. This is a serious problem of steel vessels for chemical reactions using hydrogen at high temperatures and pressure [4]. In our case, the H_2 pressures are low but, as in fusion devices, the partial pressure of H atoms is very high. Adequate remedies have been found in the steel industry. Their application to our specific problem has to be investigated if the problem of wall softening turns out to be serious.

Tritium permeation and its retention in pockets, deep in the wall might play a role on the inventory and the breeding ratio in the initial phase of operation of thermonuclear devices.

The pocket explosions are expected to lead to high local densities for short durations near the wall and may have played a role in the appearance of unipolar arcs in earlier confinement devices such as ZETA.

The model used to interpret the measurements, if correct, implies that only those surfaces which "see" the atomic ions and atoms during the plasma discharges need to be decontaminated from their bound oxyde and carbon layers. For those surfaces which are, through shadow effect, not exposed to the atomic species, thermal bake-out, to eliminate adsorbed contaminants should suffice.

It should finally be stressed that the mechanisms discussed here are not restricted in their application to the cleaning of tokamak walls. An effective cleaning can be achieved also in stellarators, high ß devices with metallic walls, mirror machines and other linear or toroidal systems.

Literature

[1] BETZ, G. et. al.
J. Appl. Phys. 45, 12 (1974), 5312

[2] DIETZ, K.J. et. al.
J. Nucl. Mat. 63 (1976) in publication

[3] KIRSCHNER, J. et. al.
Proc. 9th Symp. Fusion Tech., Garmisch 1976, p. 65

[4] KLAS, H. et. al.
Die Korrosion des Eisens und ihre Verhütung
Verlag Stahleisen M.B.H., Düsseldorf 1974

[5] KASS, W.J.
Proc. Int. Conf. Effects of Hydrogen on Behaviour of Materials, USA 1975, p. 327, ibid p. 337

[6] LOUTHAN, M.R. et. al.
ibid p. 337

[7] WEBB, R.W.
NAA-SR-10 462

[8] GRIEGER, G. et. al.
6th Europ. Conf. on Contr. Fusion and Plasma Phys.
Vol. 1, Moscow 1973, p. 101

[9] W VII A TEAM
6th Int. Conf. on Plasma Phys. and Contr. Nucl. Fusion, Berchtesgaden 1976

[10] WEGROVE, J.G.
Private communication

[11] TAYLOR, J.R.
Private communication

[12] TFR GROUP
Int. Symp. on Plasma-Wall-Interaction, Jülich 1976

[13] WAHL, G.
BBC Versuchszwischenbericht ZFL-283 (1971)

[14] HICKMOTT, T.W.
J. Chem. Phys., Vol. 32, 3 (1960) p. 810

[15] GOULD, R.K.
University of Wisconsin 1969 70-3544

[16] ORIANI, R.A.
Proc. Conf. Fundamental Aspects of Stress Corrosion Cracking, NACE, Houston 1969

[17] v. LEEUWEN, H.P.
Proc. Int. Conf. Effects of Hydrogen on Behaviour of Materials, USA 1975, p. 480

[18] BERNSTEIN, I.M. et. al.
ibid, p. 37

[19] NELSON, H.G. et. al.
Metallurgical Transactions Vol. 2, p. 953

[20] ALI KHAN, I, DIETZ, K.J., WAELBROECK, F., WIENHOLD, P.
submitted to J. Nucl. Mat.

[21] ALI KHAN, I. DIETZ, K.J. WAELBROECK, F. WIENHOLD, P.
submitted to J. Nucl. Mat.

[22] McCracken, G.M. et. al.
Int. Symp. Plasma-Wall-Interaction, Jülich 1976

[23] POSPIESZCZYK, A.
ibid

Figure Captions

fig. 1 Experimental set-up

fig. 2 Increase of the peak signals of the masses 15, 18, 27 and 28 as a function of the hydrogen pressure (for points denoted by ✓ see text)

fig. 3 Time evolution of the amplitude $V_m^p(t)$ corresponding to mass 17, and comparison with eq. (16), T_{QBP} = 300 °C

fig. 4 Typical evolution of the hydrogen pressure after pump-down following an H-atom exposure at $p_{H_2} \approx 10^{-2}$ Torr. Temperature range 40 - 180 °C.

fig. 5 Calculated production rate of hydrogen atoms in the main vessel as a function of hydrogen pressure. T_{fil} = 2000 K, S_{fil} = 20 cm^2, T_w = 442 K.

fig. 6 Calculated flux density of hydrogen atoms at the wall of the QBP as a function of the hydrogen pressure.

fig. 7 Plot of the square root $(V_{17}^p)^{1/2}$ of the amplitudes corresponding to m=17 in the presence of the test gas $p_{H_2} = 2.25 \times 10^{-5}$ as a function of the square root $(V_{17}^o)^{1/2}$ of the residual signal as the system is pumped down.

As expected from eq. (17) the variation is linear with the slope one. The points 1 and 2 were obtained in that order 16 hours later; some oxide layer appeared probably over night (diffusion or condensation) which was removed during the test.

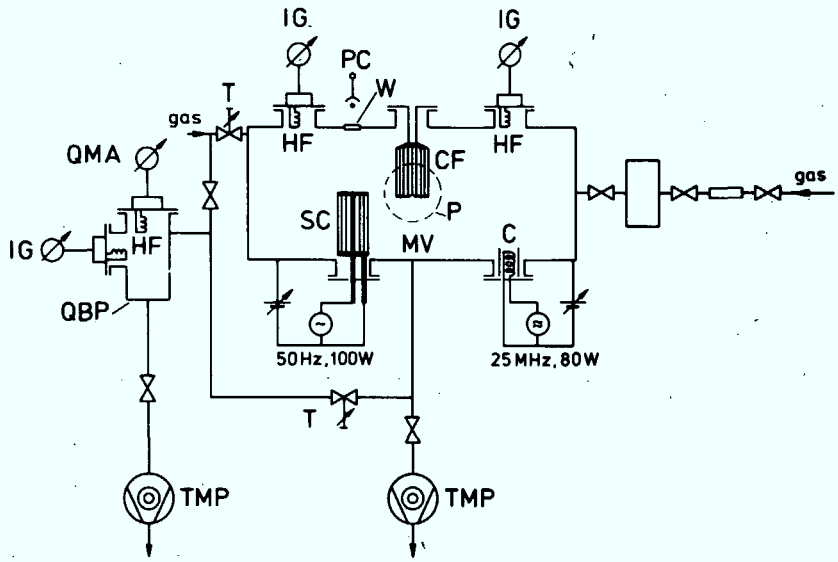

P: porthole for auger analysis
W: window
PC: photocell
T: throttle
QBP: quadrupole bypass
QMA: quadrupole mass analyzer
TMP: turbomolecular pump

MV: main vessel
SC: squirrel cage
C: rf coil
HF: hot filament
IG: ion gauge
CF: cold finger

Fig.1

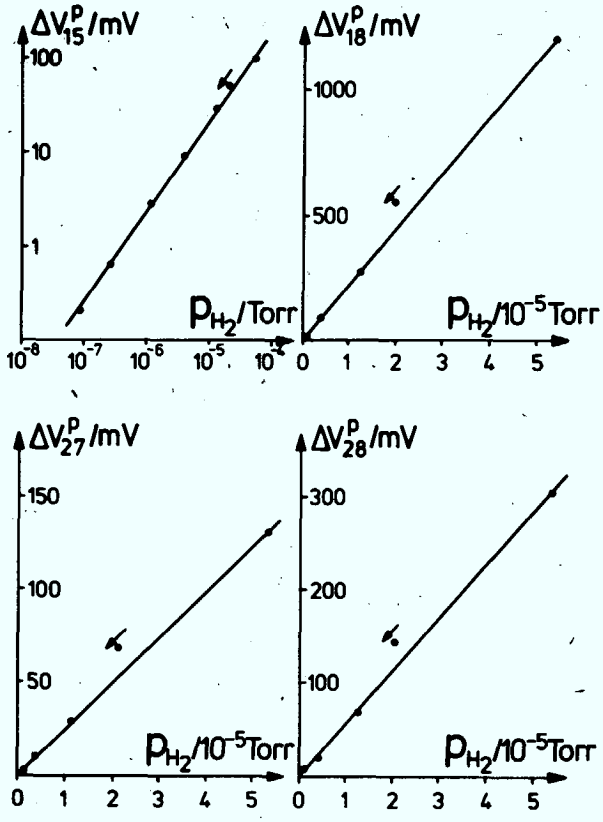
ΔV_{15}^{p}/mV
100
10
1
p_{H_2}/Torr
10^{-8} 10^{-7} 10^{-6} 10^{-5} 10^{-4}
ΔV_{18}^{p}/mV
1000
500
$p_{H_2}/10^{-5}$Torr
0 1 2 3 4 5
ΔV_{27}^{p}/mV
150
100
50
$p_{H_2}/10^{-5}$Torr
0 1 2 3 4 5
ΔV_{28}^{p}/mV
300
200
100
$p_{H_2}/10^{-5}$Torr
0 1 2 3 4 5

Fig. 2

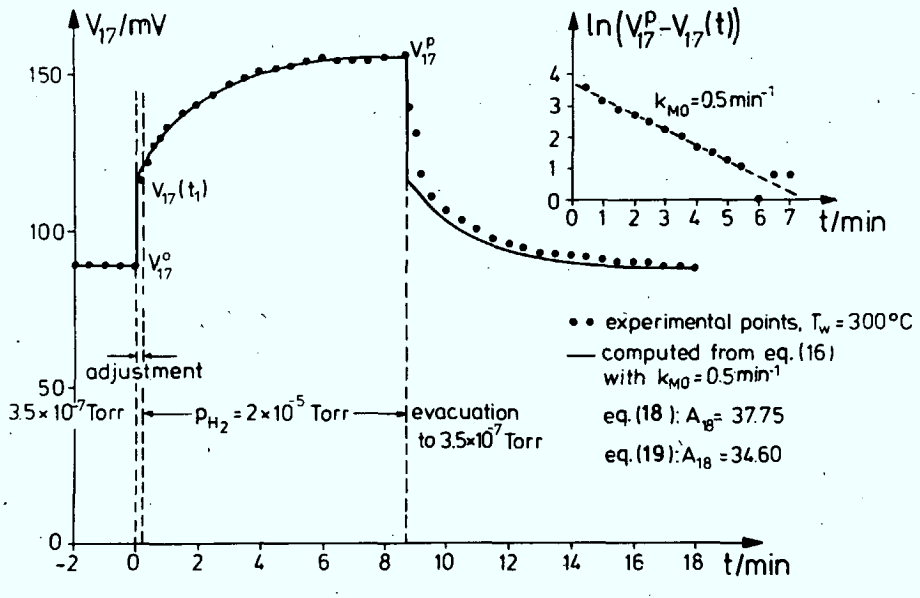
V_{17}/mV
150
100
50
0
V_{17}^{p}
$V_{17}(t_1)$
V_{17}^{o}
adjustment
3.5×10^{-7}Torr
$p_{H_2} = 2\times10^{-5}$ Torr
evacuation
to 3.5×10^{-7} Torr
-2 0 2 4 6 8 10 12 14 16 18 t/min
$\ln(V_{17}^{p}-V_{17}(t))$
4
3
2
1
0
$k_{M0}=0.5\,min^{-1}$
0 1 2 3 4 5 6 7 t/min
•• experimental points, $T_w = 300°C$
— computed from eq. (16)
with $k_{M0} = 0.5\,min^{-1}$
eq. (18): $A_{18} = 37.75$
eq. (19): $A_{18} = 34.60$

Fig. 3

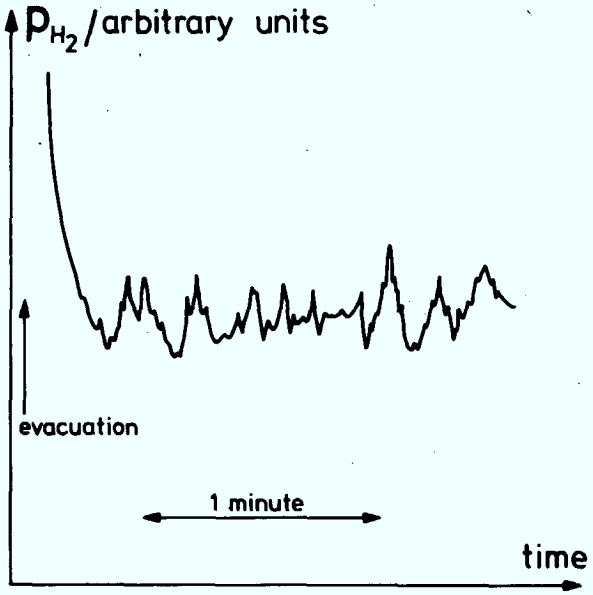
p_{H_2}/arbitrary units
evacuation
1 minute
time

Fig. 4

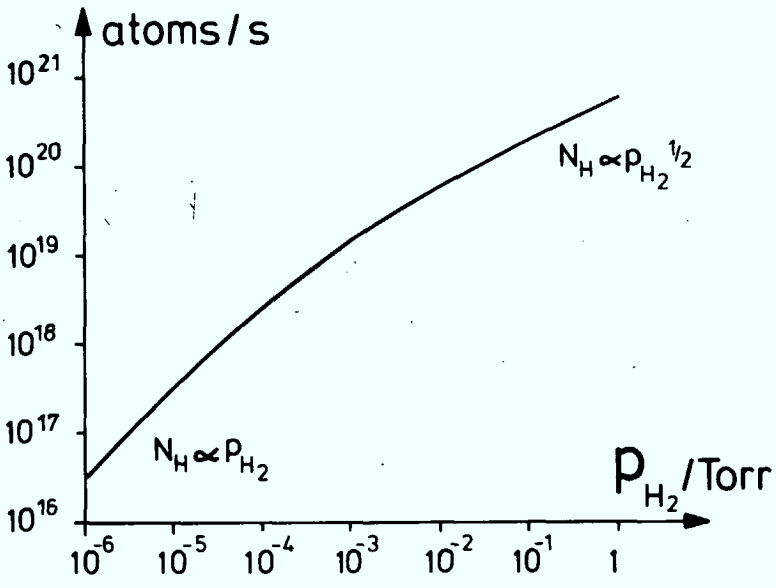
atoms/s
10^{21}
10^{20}
10^{19}
10^{18}
10^{17}
10^{16}
$N_H \propto p_{H_2}^{1/2}$
$N_H \propto p_{H_2}$
p_{H_2}/Torr
10^{-6}
10^{-5}
10^{-4}
10^{-3}
10^{-2}
10^{-1}
1

Fig. 5

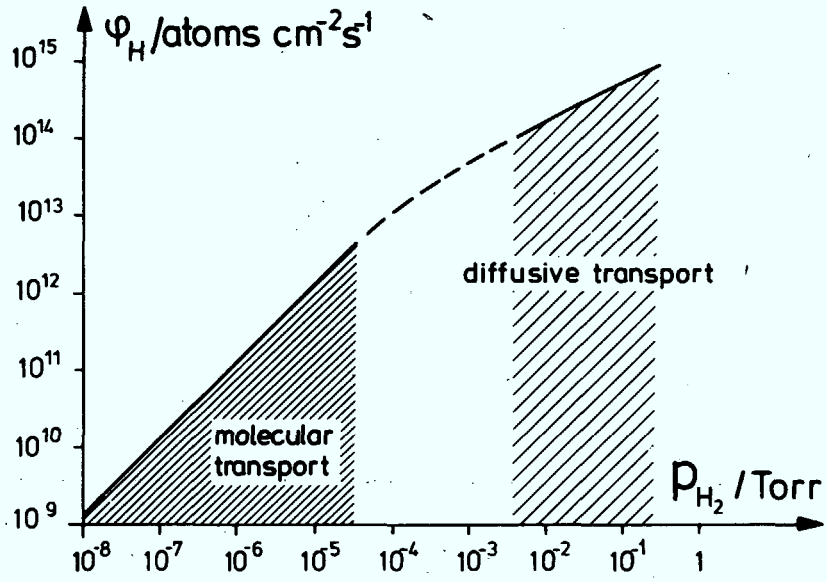
φ_H/atoms cm^{-2}s^{-1}
10^{15}
10^{14}
10^{13}
10^{12}
10^{11}
10^{10}
10^{9}
molecular transport
diffusive transport
p_{H_2} / Torr
10^{-8} 10^{-7} 10^{-6} 10^{-5} 10^{-4} 10^{-3} 10^{-2} 10^{-1} 1

Fig. 6

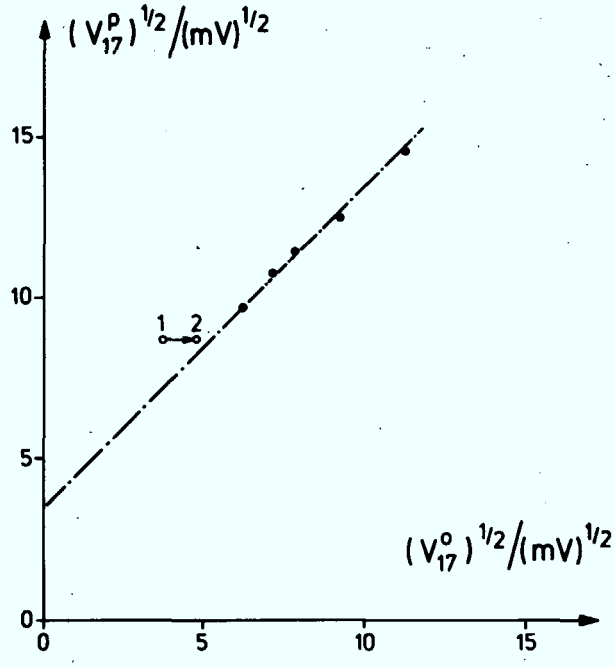
$(V_{17}^{p})^{1/2}/(mV)^{1/2}$
15
10
5
0
1 2
$(V_{17}^{o})^{1/2}/(mV)^{1/2}$
0 5 10 15

Fig. 7

Table 1

Method	$\bar{P}_{el}$ [Watt]	T_w [°C]	p_{H_2} x 10^{-2} [Torr]	Production rates x 10^{10} [$cm^{-2}s^{-1}$] m = 15	m = 18	m = 28	m = 44	Σ C x 10^{10} [$cm^{-2}s^{-1}$]	Σ O
Hot filament, 20 cm^2, 2000 K	543	217	9.5	2.0	0.2	10.1	0.2	12.3	10.7
r-f discharge	55	217	9.5	5.9	2.3	15.0	1.5	22.4	20.3
r-f and glow discharge 4 μA cm^{-2}	88	217	9.5	38.1	2.3	76.3	16.5	130.9	111.6
r-f and glow discharge 13.3 μA cm^{-2}	155	214	9.5	58.4	0.5	91.9	5.1	155.5	102.6
r-f and glow discharge 20 μA cm^{-2}	265	217	9.5	77.8	0	110.5	5.1	193.4	120.7
TFR, 100 kA, 30 kG	≈ 2000	–	≈ 0.01	0.03	0.5	0.1	0.01	0.14	0.62
TFR, discharge cleaning 22.7.76	≈10000	280–360	≈ 0.01	4.3	2.2	6.8	0.3	11.4	9.6